RSC Advances

PAPER

View Article Online
View Journal | View Issue

Cite this: *RSC Adv.*, 2025, **15**, 29217

A method for efficient separation of polystyrene nanoplastics and its application in natural freshwater

Pengju Ren, Shusheng Luo, Lijuan Wang, Yihan Chi and Yuanyuan Tang *

Nanoplastics (NPs) are an emerging contaminant in natural freshwater environments. However, there is a lack of analytical methods for separating and characterizing NPs by particle size, which is essential for analyzing their environmental behavior. Asymmetrical flow field-flow fractionation (AF4) is considered a reliable technique suitable for separating and characterizing the particle size of macromolecules, colloids, and particles. In this work, we report a method for separating and characterizing the size of polystyrene nanoplastics (PS NPs) in freshwater environments using AF4 coupled with MALS and UV-vis detectors. By optimizing the injection volume, mobile phase composition, cross-flow rate, and detector flow rate, we achieved the separation of 50 nm and 100 nm PS NPs within 40 min. The average mass recovery rate reached 88.5%, with relative standard deviations of less than 10% for different indicators in repeated measurements. The R^2 value of the linear regression between concentration and UV peak area exceeded 0.99. We applied this method to natural freshwater media and analyzed the particle sizes of particles added to the freshwater media for 0 and 48 hours using dynamic light scattering (DLS). The results revealed that, despite the appearance of a small number of particle aggregates with sizes close to 250 nm in some freshwater media after 48 hours, the optimized AF4 method still effectively separated the majority of the original unaggregated particles. This effective separation demonstrates the practical feasibility of applying the AF4 method to environmental water samples.

Received 17th January 2025
Accepted 27th July 2025

DOI: 10.1039/d5ra00409h

rsc.li/rsc-advances

1 Introduction

Global plastic production reached 430 million tons in 2023 and is anticipated to triple by 2050.[1,2] Approximately 94% of these plastics are projected to either accumulate in landfills or be discharged into the environment through processes such as surface runoff and wastewater treatment plant effluents.[2] Subsequently, these plastics undergo further fragmentation and degradation, resulting in substantial plastic debris.[3,4] Plastics degrade into fragments known as microplastics (MPs), defined as plastic particles between 1 μm and 5 mm in size. Further degradation can produce nanoplastics (NPs), typically defined as plastic particles smaller than 1 μm.[4–7] NPs possess distinctive physicochemical properties, including a large specific surface area, crystallinity, and hydrophobic surfaces, facilitating the adsorption and subsequent release of contaminants such as heavy metals, organic compounds, antibiotics, and additives like plasticizers and flame retardants.[8,9] Moreover, their reduced size presents challenges in management and increases the likelihood of entering the food chain, accumulating in top-level predators.[10–14] As a result, NPs exhibit heightened toxicity and pose elevated health risks compared to MPs.

NPs are prevalent in various environmental compartments, including rivers, lakes, oceans, sediments, and the atmosphere.[3,15–17] The initial reports on NPs date back to 2014, when Gigault *et al.* conducted laboratory simulations of the photodegradation of MPs.[18] In 2015, Halle *et al.* detected NPs in seawater samples collected from the North Atlantic Subtropical Gyre through Dynamic Light Scattering (DLS) experiments following ultrafiltration.[19] Since then, the widespread presence of MPs and NPs has been documented in freshwater systems across Europe, North America, and Asia.[20–22] Even remote areas such as the Qinghai-Tibet Plateau, Mongolia, Russia, and high mountain regions in Italy are contaminated with MPs and NPs.[23–26] Some studies suggest that the abundance of NPs may be 10^{14} times higher than MPs.[27] Despite this prevalence, it is essential to note that most detected and reported particles are still MPs, primarily due to limitations in detection methods and tools.[18] Therefore, the development of methods for the separation and characterization of NPs in real environmental contexts is of paramount importance.

Polystyrene (PS) is a prominent polymer extensively utilized across various industries, including food packaging, tableware, cosmetics, and building insulation. Polystyrene nanoplastics (PS NPs) are distinguished by their narrow particle size

Guangdong Provincial Key Laboratory of Soil and Groundwater Pollution Control, School of Environmental Science and Engineering, Southern University of Science and Technology, Shenzhen 518055, P. R. China. E-mail: tangyy@sustech.edu.cn

distribution, rendering them valuable in diverse applications such as pigments, coatings, and polymer composites.[28] As a result, PS NPs constitute a significant component of the plastics landscape.[29] A fraction of PS NPs is released in freshwater environments, exhibiting a wide range of size distributions that markedly influence their physical, chemical, and environmental behaviors.[30] On the one hand, particle size governs the behavior and transport of PS NPs in the environment.[6] Smaller particle sizes are more susceptible to microenvironmental influences in air, soil, and aqueous media and are easily absorbed and transformed by living organisms.[30] On the other hand, particle size significantly impacts the physical and chemical properties of nanoplastics.[30] The increase in specific surface area resulting from the reduction in particle size enhances the surface reactivity of NPs.[11,30] Therefore, studying the particle size of NPs is crucial for assessing their environmental impact, comprehending their properties, and developing appropriate separation techniques. Nevertheless, the small particle size and broad range of size distributions of PS NPs pose challenges in devising separation and particle size characterization methods.[8]

Various methods have been reported to separate NPs, including size exclusion and hydrodynamic chromatography.[31,32] However, when utilized for particle analysis, both methods can induce changes in sample morphology due to alterations in shear forces and may not efficiently separate particles across multiple size ranges.[33] At the nanoscale, particle size characterization can be accomplished through scanning electron microscopy (SEM), transmission electron microscopy (TEM), and dynamic light scattering (DLS).[34] Nevertheless, TEM and SEM necessitate dehydration and drying before characterization, potentially resulting in particle aggregation and deviating from the sample's original state.[34–36] Conversely, DLS instruments are unsuitable for samples with polydispersity or complex, inhomogeneous media.[37] Consequently, there is a demand for new analytical tools to address these limitations.[35] Asymmetrical flow field-flow fractionation (AF4), based on Giddings' field flow fractionation theory, has been employed to separate particles or molecules in complex mixtures.[38,39] Compared to conventional separation techniques, such as membrane filtration and liquid hydrocyclones, the AF4 method offers distinct advantages, including the ability to separate smaller particles, a broader separation range, and higher resolution in size characterization, although its sample throughput is relatively low. In addition, as a non-destructive, membrane-based, matrix-free method, AF4 avoids the need for chemicals or harsh treatments and effectively preserves test samples during the separation process, and is therefore widely used for exosomes, macromolecules and nanoparticles.[38,40–46] It has also demonstrated significant potential for separating MPs' and NPs' samples.[28,47,48] Battistini *et al.* developed a method for separating and detecting standard PS NPs samples based on an AF4 system coupled with multi-angle light scattering, providing size information on the sample particles.[28] Correia *et al.* evaluated a method for separating primary PS NPs (100 nm) in a fish tissue sample by AF4-Fluorescence.[48] Gigault *et al.* devised a programmed AF4 method to rapidly identify various submicron populations and PS NPs in unknown samples.[47] Apart from the separation mentioned above methods developed under laboratory conditions, AF4 has been applied to separate engineered nanoparticles in natural complex matrices in several studies.[49,50] Sanchez-Cachero *et al.* developed an AF4-based method for separating and characterizing platinum NPs, successfully applying it in synthetic and natural water samples.[35] Amde developed an AF4-based method for the separation and size characterization of zinc oxide NPs, demonstrating good accuracy when applied to environmental water samples.[51] Li *et al.* developed a multi-platform collaborative separation method based on AF4 for the separation, evaluation and identification of PS NPs in water.[49] It is noteworthy that, despite partial AF4 method development for PS NPs, there is still a lack of studies systematically applying and validating the feasibility of separating PS NPs in natural environmental water samples.[52]

This study focuses on optimizing and validating such an analytical method, rather than exploring new separation principles, aiming to support future environmental monitoring and research on nanoplastics. By optimizing key operational parameters and evaluating the method's performance in complex water matrices, we aim to demonstrate the practical feasibility of AF4 as a reliable analytical tool for environmental NPs research. The elution process was meticulously optimized with respect to injection concentration, carrier liquid composition, cross-flow rate, and detector flow rate. The resulting method was validated through assessments of reproducibility, recovery rates, and linearity between peak area and particle concentration. Upon validation, the method can be readily applied in future studies involving the separation of PS NPs. Although several previous studies have attempted to optimize AF4 conditions for PS NPs, systematic validation of these methods in realistic environmental water matrices—such as river water, reservoir water, and groundwater—remains limited. To address this gap, we applied the optimized AF4 method to various natural freshwater samples, with an emphasis on evaluating its robustness and performance under environmentally relevant conditions. Conventional water quality indices and DLS measurements were used to identify factors influencing AF4 separation behavior. This research contributes to a deeper understanding of both the potential and limitations of using AF4 for analyzing NPs in complex environmental settings. While the detection of naturally occurring PS NPs remains analytically challenging due to their low concentrations and the complexity of environmental matrices, this study takes a step by validating AF4's separation efficacy using spiked PS standards.

2 Materials and methods

2.1 Materials and reagents

All chemicals and reagents utilized in this study were of analytical grade. Sodium dodecyl sulfate (SDS, $C_{12}H_{25}SO_4Na$) and ammonium bicarbonate (NH_4HCO_3) were procured from Macklin (Shanghai), while sodium chloride (NaCl) was obtained from Aladdin (Shanghai). Methanol (CH_4O) was sourced from Thermo Fisher Scientific (USA). The PS NPs (50 nm and 100 nm)

were supplied by Dae Technology (China) with a particle dispersion of less than 5%. The results of dynamic light scattering (DLS) showed that for 50 nm PS NPs, the PDI was 0.04 ± 0.01, while for the 100 nm PS NPs, it was 0.01 ± 0.01, indicating relatively monodisperse distributions with low aggregation tendencies. The polyethersulfone ultrafiltration membrane, with a molecular weight cut-off (MWCO) of 30 kDa, was purchased from Jinteng (China) and employed for water filtration. Ultrapure water (UPW) was prepared using a Milli-Q gradient system (Millipore, France).

The PS NPs were characterized using a Talos F200X G2 (Thermo Fisher Scientific, USA) transmission electron microscope (TEM) operating at 200 KV. The particles' hydrodynamic diameter and zeta potential were measured using DLS with a Malvern Zetasizer Nano ZSE (Malvern Panalytical, UK). Refer to Text S1 in the SI for detailed methods and additional instrument information.

2.2 Instrument conditions and optimization of AF4 separation method

2.2.1 Instruments. The AF4 system used in this study was based on the Eclipse field-flow fractionation (FFF, Wyatt Technology, Santa Barbara, CA, USA) system. On this basis, the system combines a Wyatt's DAWN HELEOS series 18-angle laser light scattering detector (MALS), a QELS dynamic light scattering detector, a ViscoStar viscosity detector, and an rRX (dn/dc) detector for nanoparticle identification. A short channel of a trapezoidal shape was chosen for the flow channel, and the channel components were shown in Fig. S1 of SI. A spacer with a thickness of 490 μm and a regenerated cellulose (RC) membrane were selected to separate PS NPs. RC was chosen due to its low protein-binding properties, chemical stability, and minimal hydrophobic interactions with PS NPs, reducing sample loss from membrane adsorption.

In addition, a high-performance liquid chromatography (HPLC, Ultimate 3000, Thermo Fisher Scientific, USA) system was used. The system was equipped with a pump (LPG-3400SDN), an autosampler (WPS-3000TSL), and a diode array detector (DAD, DAD-3000) for UV signal detection. It was coupled with the constructed AF4 system. The sample was separated in the flow channel under the control of the autosampler and pump of the HPLC. The separated sample particles were fed into different detectors, and the signal data collected by the detectors was processed by the ASTRA 7.1.3 software (Wyatt Technology, USA). The laboratory configuration of the online AF4-MALS-UV-DAD system is illustrated in Fig. S2.

2.2.2 Optimization. In this study, we systematically optimized the operating conditions of AF4, encompassing injection volume, carrier liquid composition, cross-flow rate, and detection flow rate. Initially, PS NPs with a particle size of 50 nm (concentration of 100 mg L^{-1}) were utilized as target particles, and the injection volume was sequentially optimized at 100 μL and 1 mL. Subsequently, both PS NPs with particle sizes of 50 nm and 100 nm were chosen as target samples, ensuring their concentrations after mixing were 100 mg L^{-1} with an equal mass ratio (1 : 1).

The mobile phase composition, comprising salts, surfactants, and other chemical constituents, is a critical variable that needs careful selection for compatibility with the analyte and optimization of operational performance.[38] To identify the most compatible mobile phase composition, we compared the separation performance using two types of salt (0.5% NH_4HCO_3 and 0.01 mol per L NaCl), one type of surfactant (SDS), and ultrapure water (UPW). Additionally, the study discussed the separation effect of two different concentrations of SDS (0.005% SDS and 0.01% SDS) commonly used in mobile phases. Cross-flow rates and elution programs are other pivotal factors influencing the particle's retention time and regression particle size. Four flow rates (0.1, 0.35, 0.5, and 1 mL min^{-1}) were compared to optimize the cross-flow rate. Simultaneously, four elution programs were compared: constant, linear decay, constant then linear decay, and linear decay then constant. Finally, to examine the impact of detector flow rate variations on the separation results, three different detector flow rates were set at 0.5, 0.75, and 1 mL min^{-1}, respectively. All experiments were performed in triplicate unless otherwise specified. Quantitative data such as retention time, peak area, and recovery rate are reported as mean values ±standard deviation (SD).

2.2.3 Recovery rate. The recovery rate in this study was calculated as the mass ratio of NPs eluted during fractionation to the initial injected mass. Given the sensitivity of PS NPs to operating conditions and their propensity for adsorption onto the channel membrane surface, recovery rate evaluation and validation were crucial post-separation. The recovery was experimentally determined using a mass-sensitive UV detector. The mass recovery rate was calculated using UV peak area values in this context. The UV peak area (mAu min) obtained without focused flow and cross-flow served as a baseline for direct injection, and the mass recovery was calculated by comparing it with the UV peak area obtained during standard elution. Conforming to the ISO (International Organization for Standardization) guidelines for developing field-flow separation methods for nano-objects published in 2018, as a general rule, the recovery rate should be ≥70%.[38] In our study, a recovery rate exceeding 80% was considered acceptable.

2.2.4 Application to natural freshwater media. The separation method was further applied to natural freshwater samples collected from various sources: (1) river water from gathering areas in residential, commercial, and university town areas (Dasha River, Shenzhen City, China), (2) river water from the coastal landscape park near the outfall (Dasha River, Shenzhen City, China), (3) reservoir water from a significant water supply source and landscape reservoir (Xili Reservoir, Shenzhen City, China), and (4) groundwater samples from remote scenic spots around the county (Yinchuan City, Ningxia Hui Autonomous Region, China). The specific sampling locations are summarized in Table S1 of SI. River and reservoir water samples were collected in early February 2023, with a sampling depth of 0.5 m below the water surface. Groundwater samples were collected in late September 2022 at a depth of 30 m underground. Temperature, turbidity, and transparency were measured during field collection. To remove background particulate impurities and reduce potential interferences, all

freshwater samples were pre-filtered through a 0.22 μm polyethersulfone ultrafiltration membrane before spiking with PS NPs. Following pH measurement, the concentration of major ions (Na^+, Ca^{2+}, Mg^{2+}), total carbon (TC), and total organic carbon (TOC) were determined (Table S3 of SI). The water samples were then stored at 4 °C. PS NPs (size: 50 nm and 100 nm, concentration after mixing 100 mg L^{-1}) were introduced to the water samples and homogenized under vortex stirring to evaluate the method's applicability in natural water samples. In this study, PS NPs with particle sizes of 50 nm and 100 nm were selected because these sizes represent typical small and medium-sized NPs frequently reported in environmental research.[28,30] These particle sizes allow us to clearly investigate the influence of particle size differences on AF4 separation efficiency. A portion of the mixed sample was eluted into the AF4 system immediately (0 h assay sample), while another part was incubated in a shaker at a controlled temperature of 25 °C and a shaking speed of 200 rpm for 48 hours before elution (48 h assay sample). Additionally, each spiked sample was analyzed using DLS to validate the accuracy of the AF4 method's regression results and provide more detailed information on particle size variation in the freshwater media.

2.3 Quality control

To prevent interference caused by prolonged membrane usage, membranes were replaced after 50 uses or within one week. After replacement, new membranes were fully soaked with ultrapure water, and the system was stabilized by repeated injections before formal experiments. The flow channel was flushed with UPW for at least 1 hour before each measurement to ensure ideal conditions. During idle periods post-measurement, the flow channel was continuously flushed with 10% methanol.

3 Results and discussion

3.1 Optimization of important operating conditions for AF4 separation

Important operating conditions of AF4 were optimized in this study, such as injection volume, carrier liquid composition, cross-flow rate, and detector flow rate, which seriously affect the separation of target PS NPs. Although preliminary studies have reported the optimization of AF4 conditions for PS nanoparticles in ultrapure water, this study systematically optimized these parameters more meticulously and emphasized the applicability of the optimized method in realistic environmental media and influencing factors, clearly highlighting its practical environmental value. The operating conditions were determined according to the criteria based on signal resolution and characteristics, such as the peak intensity, the proximity of the peak base to the baseline, the degree of separation, and the particle mass recovery rate. Recovery rate was the first and most important factor to be considered and was used to determine the optimum value for all operating conditions. Peak intensity and degree of separation were evaluated based on an acceptable recovery rate. The height of the peaks judged the peak intensity, and the degree of separation was calculated by referring to the method in ISO/TS 21362:2018 (E).[38] Higher peak heights and better separations were considered to be better separations. In addition, shorter separation time is also a factor to be considered.

First, the injection volume was optimized. As shown in Fig. S3, in the continuous injection of two different concentrations of PS NPs, the sample peak morphology was good at an injection volume concentration of 50 μL. Therefore, a 50 μL injection volume was adopted in this study, with the actual analyte concentration set at 0.005 g L^{-1}, aligning with conclusions from numerous studies.[53] As a rule, the analyte concentration should not exceed 1 g L^{-1}.[38] However, this value only serves as a broad upper limit to initiate the optimization process, and optimal concentrations can often be much lower, which was supported by the results of our study.[38] A flat-head peak with missing peak information emerged at an injection volume concentration of 1 mL. This observation aligns with the findings of Sun *et al.*, who also noted flat-head peaks for the nanoparticulate matter at an injection volume of 1 mL.[54] The probable cause was the excessively high concentration of PS NPs, surpassing the detection range of the UV-DAD detector. Despite the value of the recovery rate indicating that the 1 mL injection volume provided a better recovery rate, the recovery rate corresponding to a 50 μL injection volume met the requirements of common studies.[38]

Next, in comparing four mobile phase compositions, SDS emerged as the most compatible, with 0.01% SDS providing the highest signal intensity, optimal recovery, and shortest separation time. Among tested mobile phase compositions (Fig. 1a), UPW resulted in the lowest recovery and longest elution time, accompanied by peak tailing. The presence of tailing may be attributed to the strong interaction between the membrane and the PS NPs, necessitating the addition of other chemical components to weaken this interaction. Moreover, adding two salts improved the recovery of the target PS NPs, particularly 0.01 mol per L NaCl, which resulted in a peak pattern adhering to a normal distribution and achieved good separation. However, using NaCl with UPW as the mobile phase weakened the peak signal, and based on the zeta potential detection results of PS NPs, the particles in aqueous solution generally carry a negative charge. The dissociation of NaCl released many positively charged sodium ions, acting as a bridging agent for PS NPs and potentially triggering aggregation. Several studies have indicated that, despite the low concentration of NaCl, they may still induce the aggregation of PS NPs.[55,56]

Third, the cross-flow rate was optimized and is shown in Fig. 1b. Cross-flow rates of 0.1 mL min^{-1} caused rapid elution and poor recovery, while 1 mL min^{-1} resulted in overly prolonged elution. This aligns with the theory of asymmetric field flow separation, where an increased cross-flow rate exerts a more significant force on particles perpendicular to the flow channel, leading to a more dispersed distribution and wider peak exit time for particles of different sizes in the flow channel.[39] The experimental results of mass recovery indicated

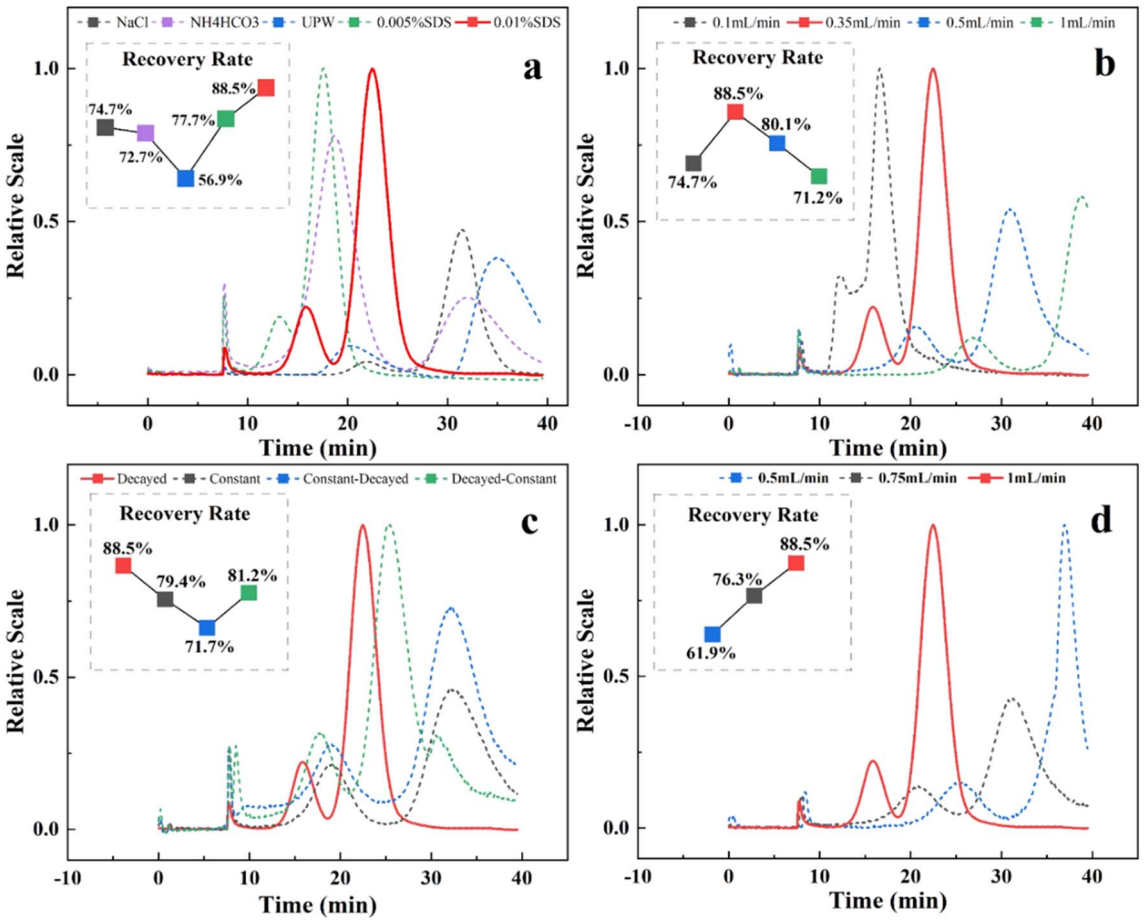

Fig. 1 Optimization results of carrier liquid composition (a), cross-flow rate (b), cross-flow rate variation method (c) and detector flow rate (d). In the carrier liquid composition, the recovery rates of NaCl, NH_4HCO_3, UPW, 0.005% SDS and 0.01% SDS were 74.7 ± 2.3%, 72.7 ± 4.5%, 56.9 ± 8.9%, 77.7 ± 5.6%, 88.5 ± 0.3%, respectively; in the cross-flow rate, the recovery rates of 0.1, 0.35, 0.5 and 1 mL min^{-1} were 74.7 ± 4.2%, 88.5 ± 0.3%, 80.1 ± 1.6% and 71.2 ± 2.6%, respectively; in the cross-flow rate variation method, the recovery rates of decayed, constant, constant-decayed and decayed-constant were 88.5 ± 0.3%, 79.4 ± 1.1%, 71.7 ± 6.6% and 81.2 ± 4.2%, respectively; in the detector flow rate, the recovery rates of 0.5, 0.75 and 1 mL min^{-1} were 61.9 ± 12.3%, 76.3 ± 2.1% and 88.5 ± 0.3%, respectively.

that a cross-flow rate of 0.35 mL min^{-1} yielded the highest recovery rate for the target PS NPs. Subsequently, mass recovery gradually decreased as the cross-flow rate increased further, consistent with the findings of Sun *et al.*[54] It is suggested that a high cross-flow rate concentrates some larger particles on the surface of the channel membrane. This concentration intensifies particle–membrane interaction, reducing particle recovery rates and potentially causing membrane clogging or contamination, thereby shortening the service life of the channel membrane.[38,57] The decrease in peak height observed when the cross-flow rate exceeded 0.5 mL min^{-1} further supports the loss of particle mass recovery. This behavior is consistent with AF4 separation theory, where smaller particles with higher diffusion coefficients elute earlier due to their equilibrium at higher channel positions under laminar flow. Considering these factors, a cross-flow rate of 0.35 mL min^{-1} was chosen to separate the target PS NPs.

Building upon the optimized cross-flow rate, we further refined the cross-flow rate variation method, and the results are depicted in Fig. 1c. The linearly decaying cross-flow variation method exhibited stronger signal intensity, better separation, higher recovery rate, and shorter retention time, making it more suitable for the separation of PS NPs with particle sizes of 50 and 100 nm. This outcome aligns with the recommendations for elution procedure optimization in the ISO standard.[38] According to ISO, an attenuated cross-flow rate facilitates the rapid elution of components when the dynamic range of component sizes to be separated is significant.[38] In contrast, a constant cross-flow rate is recommended for smaller size ranges.[38] The notable contrast between the high peak intensity and recovery associated with decay and the lower values for a constant cross-flow rate suggests that the 50 nm particle size difference already falls within the range of significant differences in fraction sizes when using AF4 for PS NPs separation. Therefore, the use of a decaying cross-flow rate should be considered judiciously. On the other hand, the decay followed by a constant variation appears to be a more promising direction for cross-flow rate optimization. Despite some distortion in peak tails, the higher signal intensities and recoveries lead us to believe that continued optimization of the remaining

parameters under this cross-flow rate variation may yield improved separation results.

The detector flow rate, which influences the retention time, was also considered. As depicted in Fig. 1a and d lower detector flow rate (0.5 mL min^{-1}) caused a delay in the sample peak and prolonged the elution time. On the other hand, an increase in the flow rate advanced the sample peak and reduced separation, with a detector flow rate of 1 mL min^{-1} providing more appropriate separation and elution time. Concurrently, experimental recovery results demonstrated a gradual increase in the recovery rate with an incremental rise in the detector flow rate. Consequently, 1 mL min^{-1} was selected as the optimal detector flow rate.

Therefore, this study utilized a constant focus flow rate of 1 mL min^{-1} and a focus time of 5 minutes, consistent with the approach adopted in numerous studies, including an AF4 separation study on PS NPs.[47,53] Following the optimization of the parameters mentioned above, the optimal AF4 operating conditions and elution steps are summarized in Table 1, and the separation results are presented in Fig. 2.

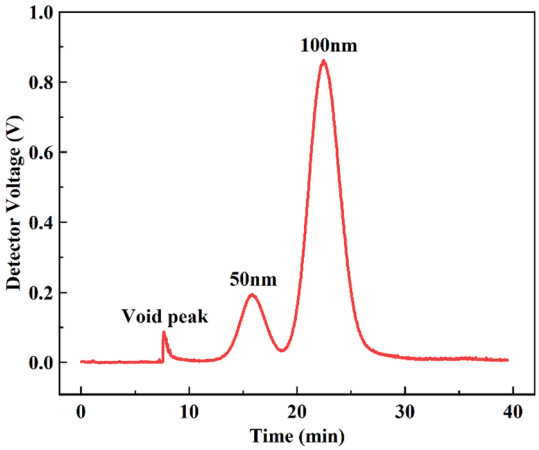

Fig. 2 Optimization results of the AF4 method for separating PS NPs.

3.2 Validation of AF4 separation method

To validate the accuracy of the particle sizes, TEM images of 50 nm and 100 nm PS NPs were obtained and are presented in Fig. 3a and b, showing that both particles are close to spherical in shape. Relatively uniform particle size distributions were observed, although a few of them had significant size variations, which is consistent with the results of the DLS tests shown in Fig. 3c. Regarding the results of the particle size calculations in Table S2, the AF4 method exhibited the most minor variability with the TEM, particularly at the larger particle sizes of 100 nm PS NPs, where the variability was less than 1%. Although DLS is widely used in nanoscale studies, the results of this work suggest that DLS may give relatively high results for particle size analysis at the nanoscale, similar to the findings of some other scholars.[51,58–60]

Meanwhile, the reliability of the established method was also validated through repeatability experiments, particle mass recovery rate, and the degree of response of peak area *versus* concentration. Repeatability experiments were performed in AF4 twice a day for three consecutive days, both in the morning (9:00) and evening (17:00). The method's repeatability was assessed by calculating the relative standard deviations (RSD, %) of the retention time (R_t, min), MALS regression radius (R_g, nm) values, and UV peak areas (mAu min). As shown in Table S3 and Fig. 3d, satisfactory peak shapes were obtained after six repeatability experiments, and the particles' mass recovery rates were all over 85%. The RSD values for all parameters were less than 10%, especially for R_t, indicating the robust reproducibility of our established AF4 separation method. The maximum RSD values for R_g and UV peak area did not exceed 5.6%, adhering to ISO guidelines and falling within an acceptable range.[28,38] Notably, the RSD values for the R_g corresponding to 100 nm PS NPs were less than 1%, indicating the potential and advantage of AF4 in separating nanoparticles with slightly larger particle sizes.

The degree of response of the UV peak area to concentration was employed to characterize the relationship between the UV absorption signal and the sample concentration in field flow separation. Such elution behavior is fundamentally governed by the AF4 principle, where particle retention is inversely related to diffusion coefficient, allowing smaller particles to migrate faster in the channel. According to the Lambert–Beer law, UV absorption exhibits a linear relationship with the substance

Table 1 Optimal AF4 operating conditions and elution steps

Parameter	Time (min)	Value
Material		PS NPs (50 100 nm)
Carrier solution		0.01% SDS
Membrane type		Regenerated cellulose; cut-off 10 kDa
UV-VIS wavelength		254 nm
Inject volume		50 μL
Spacer thickness		490 μm
Run time		40 min
Elution steps		
Elution	1	Detector flow 1.00 mL min^{-1} (constant)
Focus	1	Focus flow 1.00 mL min^{-1} (constant)
Focus and inject	5	Focus flow 1.00 mL min^{-1} (constant); inject flow 0.2 mL min^{-1} (constant)
Elution	30	Cross-flow 0.35–0 mL min^{-1} (linear decay)
Elution and inject	3	Detector flow 1.00 mL min^{-1} (constant)

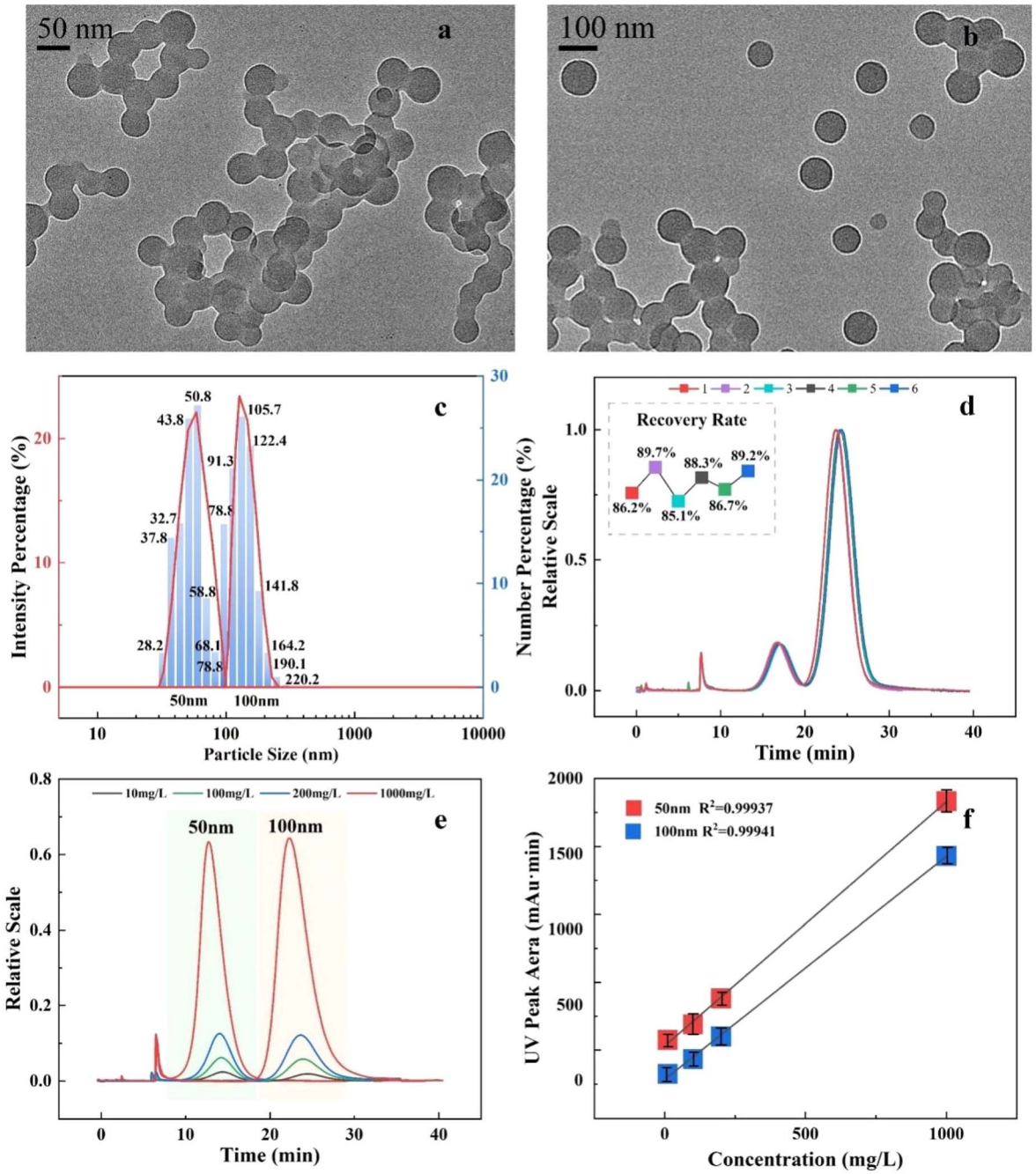

Fig. 3 Validation results of the optimized AF4 method for the separation of PS NPs (a) and (b) TEM images of 50 nm (a) and 100 nm (b) particles; (c) particle size and distribution measured by DLS; (d) six replicate elutions using the optimized AF4 method over three days; (e) and (f) UV detection signal of UV-DAD at different concentrations (e) and linear fit results of UV peak area and concentration (f).

concentration within a specific concentration range. For continuous injection, this study chose 50 nm and 100 nm PS NPs at increasing concentrations (10, 100, 200, 1000 mg L^{-1}). The degree of response of UV peak area to concentration was assessed by fitting the R^2 value of the linear relationship between the UV absorption signal measured by the UV-DAD detector and the injection concentration. As illustrated in Fig. 3e and f, all R^2 values for the linear fits exceeded 0.99, signifying the excellent reliability of the optimized method and the AF4 system for the UV signal across varying analyte concentrations.

The limits of detection (LoD) and quantification (LoQ) for the AF4 method were determined based on three mass-flow fractograms obtained from measuring a PS NPs mix sample (1–100 mg L^{-1}, 50 nm and 100 nm). Following the approach used by Meermann *et al.*, the average peak broadness and peak heights were derived from the respective mass-flow fractograms, which were considered as background values[70]. The

standard deviation of the background noise was calculated by repeating the experiment three times, with LoD being obtained by multiplying the standard deviation by a factor of 3, and LoQ by multiplying it by 10. Accordingly, the LoD for 50 nm particles was 9.3 μg mL^{-1}, while for 100 nm particles, it was 20.1 μg mL^{-1}. The LoQ for 50 nm particles was 31 μg mL^{-1}, and for 100 nm particles, it was 67 μg mL^{-1}. These values highlight the sensitivity of the AF4-MALS-UV method for PS detection in environmental samples.

3.3 Application of the AF4 method to the separation of PS NPs in freshwater media

It should be emphasized that the PS particles used in this section were artificially introduced into natural freshwater samples. This study did not attempt to detect PS particles already present in environmental media, but rather to evaluate the applicability of the AF4 system for separating and characterizing such particles in real-world water matrices. After applying the AF4 method in freshwater media, the results in Fig. 4 show that the PS NPs added in different freshwater media can be effectively separated by the AF4 method. At 0 h, the peak patterns exhibited good reproducibility, with relatively small differences in the particle size regression results, particularly for the 100 nm PS NPs particles. The RSD of the particle size regression was only 0.92% for 100 nm PS NPs compared to 2.82% for 50 nm PS NPs. After 48 hours of shaking, the central part of the peak pattern was well-formed, and the two peaks could still be separated without obvious overlap. The RSD of the size regression results remained below 10%, affirming the accuracy of the AF4 method in nano-scale particle size calculation and its broad applicability in complex environments. The morphology of the sample fractograms, along with the signal intensity provided by MALS, indicated that the better resolution followed the order of landscape park river water (SZB) > groundwater (YCG) > landscape reservoir water (XLR) > river water in populated areas (DSR). The smallest

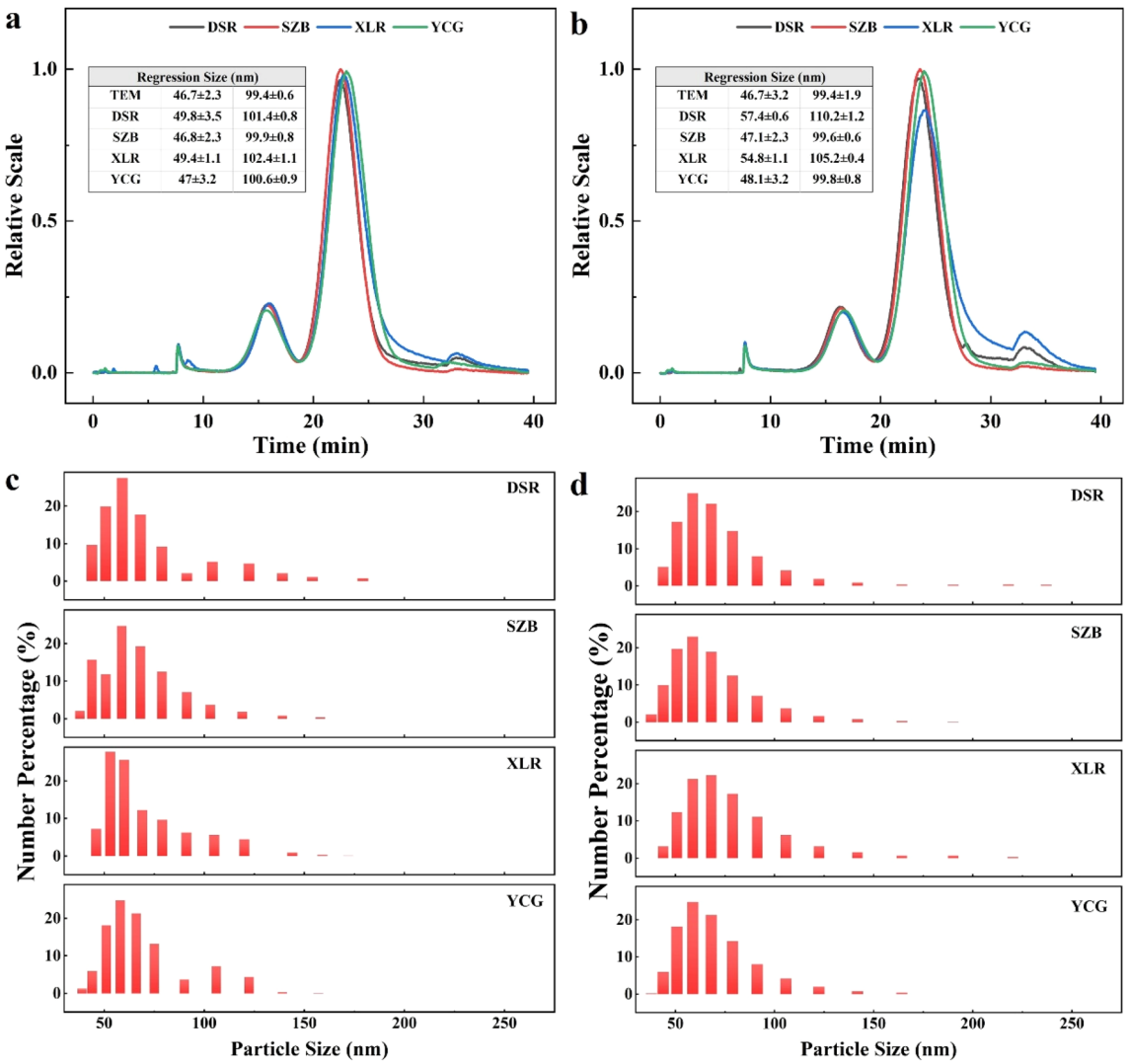

Fig. 4 Results of applying the AF4 method to separate PS NPs added to different freshwater (0 h (a) and 48 h (b), DSR: Dasha river; SZB: Shenzhen bay; XLR: Xili reservoir; YCG: Yinchuan groundwater) and the results of the particle size types and percentages (0 h (c) and 48 h (d)) given by the DLS.

tail bulge and the strongest signal strength suggested that the optimized AF4 method provides the best resolution for SZB. The results of particle size regression were compared with TEM, showing the best consistency for SZB. The separation effect for groundwater represented by YCG was slightly weaker than that of SZB but significantly better than that of river in populated areas (DSR) and landscape reservoir (XLR). The separation effect of reservoir water was the least effective; after 48 h, there was a significant decrease in the MALS signal peak corresponding to 100 nm. This phenomenon was observed only in the separation of reservoir water. Additionally, the tail of the fractograms corresponding to XLR exhibited a bulge, and although this bulge was present in all freshwater bodies, it seemed most pronounced in reservoir water.

Regarding the cause of the bulge at the end of the fractogram, we ruled out the effects of prolonged use of the liquid chromatographic column, overloading due to high injection concentration, and excessive use of the membrane. Upon comparing with the results of DLS, we believe the tail bulge may be related to some large-size aggregates in the water. The DLS results (Fig. 4c) showed that even the PS NPs particles just added to water still exhibited slight aggregation during the elution process, with all water bodies showing aggregates with a particle size over 150 nm, particularly in DSR, where aggregates with a particle size of 179 nm were observed. After 48 hours, as shown in Fig. 4d, 0.3% of aggregates with a particle size of 237 nm appeared in DSR water, while 0.3% of aggregates with a particle size of 220 nm appeared in XLR water. Later, these larger aggregates were eluted, forming a slight bulge on the fractal map. We believe that this part of the aggregates may originate from the aggregation behavior of the 50 nm size PS NPs. Numerous studies have demonstrated that smaller PS NPs are more prone to aggregate under the same conditions.[56,61] Meanwhile, zeta potential assays of PS NPs indicate that particles with a particle size of 100 nm have more negative zeta potential values in the UPW media (Table S2), suggesting that 100 nm particles exhibit better stability.

PS NPs are separated differently in freshwater media based on pH, electrolyte type and concentration, and organic matter content.[35,62] The solution's pH influences the ionization and surface charge of functional groups on PS NPs, which in turn affects the extent of electrostatic repulsion and aggregation behavior.[63] Previous studies have demonstrated that PS NPs maintain a negative charge across a broad pH range of 2.3–11.1.[63–65] Consequently, in aquatic environments, PS NPs can achieve stabilization through electrostatic repulsion, with stability generally rising with an increase in pH.[65] In our investigation, the pH of all freshwater media approximated 7.3 (Table S4 of SI), indicating weak alkalinity.[65] Simultaneously, zeta potential detection revealed the negative charge of PS NPs (Table S2), enhancing particles' stability and facilitating the application of AF4 in freshwater environments. Furthermore, the charge carried by ions in the aqueous media reduces the particles' stability and contributes to aggregation.[66] Previous research indicates that the critical concentration for rapid particle coalescence is inversely proportional to the sixth power of ionic charge, with divalent ions exerting 50–83 times more influence than monovalent ions.[67,68] Our investigation scrutinized monovalent, divalent, and trivalent metal cations in freshwater systems, revealing minimal detection of metal cations except Na^+, Mg^{2+}, and Ca^{2+}. SZB water samples exhibited elevated concentrations of Na^+ and Mg^{2+}, while YCG samples showed relatively high levels of Na^+ and Ca^{2+}. Surprisingly, compared to DSR and XLR, the application of AF4 in SZB and YCG yielded superior fractal plots and particle size regression results. This phenomenon suggests that monovalent and divalent cations in the appropriate concentration ranges do not have a very significant effect on PS NPs in AF4 separation. The low response of the AF4 method to ion concentration allows its application in aqueous media with varying salinities. Meanwhile, our results demonstrate that AF4 can effectively separate nanoparticles based on their predominant size, even in a small number of aggregates. High TC concentrations did not influence separation, although a rise in TOC seemed to affect the particle signal strength in the solution. In Sanchez-Cachero *et al.*'s investigation, larger particles of 30 nm demonstrated an increase in signal intensity in solutions with high TOC contents.[35] This was supported by the fact that the signal strength of PSNPs in SZB water bodies was higher than that of DSR at both 0 h and 24 h in this investigation. However, since there was no significant difference in TOC concentration between the selected water bodies, this idea needs to be further verified and investigated by other scholars.

Compared to previous studies employing AF4 for nanoparticle separation in environmental samples, our findings align well with existing reports.[51,69] Our work expands on these foundational studies by systematically optimizing AF4 parameters specifically for PS NPs, validating its reproducibility and effectiveness across diverse freshwater samples, thus contributing additional evidence on AF4's practicality for environmental nanoplastic monitoring.

4 Conclusions

This work provides a validated analytical protocol for PS NPs separation and characterization in natural freshwater environments. The optimization of various factors within the AF4 system proved essential in achieving reproducible results and satisfactory recoveries of PS NPs. The 0.01% SDS + UPW combination showed more significant advantages in mobile phase optimization. Meanwhile, the size and variation of the cross-flow rate greatly affect the results of optimization. In this study, we validated the AF4-MALS-UV method specifically for separating PS NPs in complex freshwater environments. By analyzing the physicochemical properties of different water samples, we successfully identified critical factors affecting the separation performance, contributing valuable methodological insights for future environmental applications. In general, the proposed method can be used for separating and characterization PS NPs in natural freshwater, as well as the possibility to be expanded to other complex aqueous media.

While the proposed AF4 method demonstrated effective separation and characterization of PS NPs in various freshwater environments, certain limitations remain. This study focused

on spiked PS NPs rather than naturally occurring nanoplastics, which typically exist at lower concentrations and exhibit more complex compositions. Additionally, the method relies on AF4-MALS-UV without combining chemical identification techniques. Future research should explore applying the optimized method in long-term field monitoring and testing its compatibility with other analytical tools, such as Raman spectroscopy, to enhance environmental nanoplastics analysis.

Conflicts of interest

There are no conflicts to declare.

Data availability

The data supporting this article have been included as part of the SI.

The SI is available, including one text, three figures, and four tables. See DOI: **https://doi.org/10.1039/d5ra00409h**.

Acknowledgements

The authors are grateful to the Natural Science Foundation of Guangdong Province (2021B1515020041), National Natural Science Foundation of China (42277403), Projects of International Cooperation and Exchange of the National Natural Science Foundation of China (NSFC-UNEP: 32261143459), Guangdong Provincial Key Laboratory of Soil and Groundwater Pollution Control (No. 2023B1212060002), and High-level University Special Fund (G03050K001) for financial support. Also, we want to thank the Center for Computational Science and Engineering at Southern University of Science and Technology (SUSTech), and core research facilities at SUSTech to provide quality resources and services.

References

1 United Nations Environment Programme, *World Environment Day brings solutions to plastic pollution into focus*, 2023, **https://www.unep.org/news-and-stories/press-release/world-environment-day-brings-solutions-plastic-pollution-focus**.

2 T. Thompson, Plastic pollution: Three problems that a global treaty could solve, *Nature*, 2022, DOI: **10.1038/d41586-022-03835-w**.

3 C. G. Alimba and C. Faggio, Microplastics in the marine environment: Current trends in environmental pollution and mechanisms of toxicological profile, *Environ. Toxicol. Pharmacol.*, 2019, **68**, 61–74, DOI: **10.1016/j.etap.2019.03.001**.

4 O. S. Alimi, J. Farner Budarz, L. M. Hernandez and N. Tufenkji, Microplastics and nanoplastics in aquatic environments: Aggregation, deposition, and enhanced contaminant transport, *Environ. Sci. Technol.*, 2018, **52**(4), 1704–1724, DOI: **10.1021/acs.est.7b05559**.

5 F. Gagne, Detection of polystyrene nanoplastics in biological tissues with a fluorescent molecular rotor probe, *J. Xenobiot.*, 2019, **9**(1), 1–3, DOI: **10.4081/xeno.2019.8147**.

6 K. Mattsson, L. A. Hansson and T. Cedervall, Nano-plastics in the aquatic environment, *Environ. Sci.: Processes Impacts*, 2015, **17**(10), 1712–1721, DOI: **10.1039/c5em00227c**.

7 A. Ter Halle, L. Ladirat, M. Martignac, A. F. Mingotaud, O. Boyron and E. Perez, To what extent are microplastics from the open ocean weathered?, *Environ. Pollut.*, 2017, **227**, 167–174, DOI: **10.1016/j.envpol.2017.04.051**.

8 N. Kokilathasan and M. Dittrich, Nanoplastics Detection and impacts in aquatic environments – A review, *Sci. Total Environ.*, 2022, **849**, 157852, DOI: **10.1016/j.scitotenv.2022.157852**.

9 A. M. Elgarahy, A. Akhdhar and K. Z. Elwakeel, Microplastics prevalence, interactions, and remediation in the aquatic environment: A critical review, *J. Environ. Chem. Eng.*, 2021, **9**(5), DOI: **10.1016/j.jece.2021.106224**.

10 T. Cedervall, L. A. Hansson, M. Lard, B. Frohm and S. Linse, Food chain transport of nanoparticles affects behaviour and fat metabolism in fish, *PLoS One*, 2012, **7**(2), DOI: **10.1371/journal.pone.0032254**.

11 S. A. Strungaru, R. Jijie, M. Nicoara, G. Plavan and C. Faggio, Micro- (nano) plastics in freshwater ecosystems: Abundance, toxicological impact and quantification methodology, *Trac. Trends Anal. Chem.*, 2019, **110**, 116–128, DOI: **10.1016/j.trac.2018.10.025**.

12 Z. Yan, Y. Liu, T. Zhang, F. Zhang, H. Ren and Y. Zhang, Analysis of microplastics in human feces reveals a correlation between fecal microplastics and inflammatory bowel disease status, *Environ. Sci. Technol.*, 2021, **56**(1), 414–421, DOI: **10.1021/acs.est.1c03924**.

13 H. A. Leslie, M. J. M. van Velzen, S. H. Brandsma, A. D. Vethaak, J. J. Garcia-Vallejo and M. H. Lamoree, Discovery and quantification of plastic particle pollution in human blood, *Environ. Int.*, 2022, **163**, DOI: **10.1016/j.envint.2022.107199**.

14 A. R. Aves, L. E. Revell, S. Gaw, H. Ruffell, A. Schuddeboom, N. E. Wotherspoon, M. LaRue and A. J. McDonald, First evidence of microplastics in Antarctic snow, *Cryosphere*, 2022, **16**(6), 2127–2145, DOI: **10.5194/tc-16-2127-2022**.

15 A. L. Andrady, Microplastics in the marine environment, *Mar. Pollut. Bull.*, 2011, **62**(8), 1596–1605, DOI: **10.1016/j.marpolbul.2011.05.030**.

16 F. Gao, J. Li, C. Sun, L. Zhang, F. Jiang, W. Cao and L. Zheng, Study on the capability and characteristics of heavy metals enriched on microplastics in marine environment, *Mar. Pollut. Bull.*, 2019, **144**, 61–67, DOI: **10.1016/j.marpolbul.2019.04.039**.

17 D. Eerkes-Medrano, R. C. Thompson and D. C. Aldridge, Microplastics in freshwater systems: A review of the emerging threats, identification of knowledge gaps and prioritisation of research needs, *Water Res.*, 2015, **75**, 63–82, DOI: **10.1016/j.watres.2015.02.012**.

18 J. Gigault, B. Pedrono, B. Maxit and A. Ter Halle, Marine plastic litter: the unanalyzed nano-fraction, *Environ. Sci. Nano*, 2016, **3**(2), 346–350, DOI: **10.1039/c6en00008h**.

19 A. Ter Halle, L. Jeanneau, M. Martignac, E. Jardé, B. Pedrono, L. Brach and J. Gigault, Nanoplastic in the north atlantic subtropical gyre, *Environ. Sci. Technol.*, 2017, **51**(23), 13689–13697, DOI: **10.1021/acs.est.7b03667**.

20 R. Dris, J. Gasperi, V. Rocher, M. Saad, N. Renault and B. Tassin, Microplastic contamination in an urban area: a case study in Greater Paris, *Environ. Chem.*, 2015, **12**(5), 592–599, DOI: **10.1071/en14167**.

21 S. A. Carr, J. Liu and A. G. Tesoro, Transport and fate of microplastic particles in wastewater treatment plants, *Water Res.*, 2016, **91**, 174–182, DOI: **10.1016/j.watres.2016.01.002**.

22 K. Liu, X. Wang, T. Fang, P. Xu, L. Zhu and D. Li, Source and potential risk assessment of suspended atmospheric microplastics in Shanghai, *Sci. Total Environ.*, 2019, **675**, 462–471, DOI: **10.1016/j.scitotenv.2019.04.110**.

23 X. Xiong, K. Zhang, X. Chen, H. Shi, Z. Luo and C. Wu, Sources and distribution of microplastics in China's largest inland lake - Qinghai Lake, *Environ. Pollut.*, 2018, **235**, 899–906, DOI: **10.1016/j.envpol.2017.12.081**.

24 C. M. Free, O. P. Jensen, S. A. Mason, M. Eriksen, N. J. Williamson and B. Boldgiv, High-levels of microplastic pollution in a large, remote, mountain lake, *Mar. Pollut. Bull.*, 2014, **85**(1), 156–163, DOI: **10.1016/j.marpolbul.2014.06.001**.

25 H. K. Imhof, N. P. Ivleva, J. Schmid, R. Niessner and C. Laforsch, Contamination of beach sediments of a subalpine lake with microplastic particles, *Curr. Biol.*, 2013, **23**(19), R867–R868, DOI: **10.1016/j.cub.2013.09.001**.

26 E. S. Kazak, E. A. Filimonova and A. E. Preobrazhenskaya, Occurrence and detection problems of micro- and nanoplastics in the water environment of Russia, *Mosc. Univ. Geol. Bull.*, 2023, **78**(1), 110–123, DOI: **10.3103/s0145875223010076**.

27 M. Enfrin, J. Lee, Y. Gibert, F. Basheer, L. Kong and L. F. Dumée, Release of hazardous nanoplastic contaminants due to microplastics fragmentation under shear stress forces, *J. Hazard. Mater.*, 2020, **384**, 121393, DOI: **10.1016/j.jhazmat.2019.121393**.

28 B. Battistini, F. Petrucci and B. Bocca, In-house validation of AF4-MALS-UV for polystyrene nanoplastic analysis, *Anal. Bioanal. Chem.*, 2021, **413**(11), 3027–3039, DOI: **10.1007/s00216-021-03238-2**.

29 California Against Waste, List of california jurisdiction with polystyrene ordinances, CAWrecycles org, Retrieved October 26, 2023, **https://www.cawrecycles.org/polystyrene-local-ordinances**.

30 J. Gigault, H. El Hadri, B. Nguyen, B. Grassl, L. Rowenczyk, N. Tufenkji, S. Y. Feng and M. Wiesner, Nanoplastics are neither microplastics nor engineered nanoparticles, *Nat. Nanotechnol.*, 2021, **16**(5), 501–507, DOI: **10.1038/s41565-021-00886-4**.

31 A. Richard, S. A. S. Cave, M. J. Gidley and R. G. Gilbert, Characterization of starch by size-exclusion chromatography: The limitations imposed by shear scission, *Biomacromolecules*, 2009, **10**, 2245–2253, DOI: **10.1021/bm900426n**.

32 J.-G. Choi, M. Hasan, H. Akter and S.-S. Lee, Characterization of dextran-coated magnetic nanoparticles (Fe_3O_4) conjugated with monoclonal antibody through low gradient magnet and centrifugation-based buffer separation processes, *Curr. Appl Phys*, 2023, **48**, 79–83, DOI: **10.1016/j.cap.2023.01.010**.

33 P. Guo, Y. Li, J. An, S. Shen and H. Dou, Study on structure-function of starch by asymmetrical flow field-flow fractionation coupled with multiple detectors: A review, *Carbohydr. Polym.*, 2019, **226**, 115330, DOI: **10.1016/j.carbpol.2019.115330**.

34 F. Laborda, E. Bolea, G. Cepria, M. T. Gomez, M. S. Jimenez, J. Perez-Arantegui and J. R. Castillo, Detection, characterization and quantification of inorganic engineered nanomaterials: A review of techniques and methodological approaches for the analysis of complex samples, *Anal. Chim. Acta*, 2016, **904**, 10–32, DOI: **10.1016/j.aca.2015.11.008**.

35 A. Sanchez-Cachero, S. Lopez-Sanz, N. R. Farinas, A. Rios and R. Martin-Doimeadios, A method based on asymmetric flow field flow fractionation hyphenated to inductively coupled plasma mass spectrometry for the monitoring of platinum nanoparticles in water samples, *Talanta*, 2021, **222**, 121513, DOI: **10.1016/j.talanta.2020.121513**.

36 S. Lopez-Sanz, F. J. Guzman Bernardo, R. C. Rodriguez Martin-Doimeadios and A. Rios, Analytical metrology for nanomaterials: Present achievements and future challenges, *Anal. Chim. Acta*, 2019, **1059**, 1–15, DOI: **10.1016/j.aca.2019.02.009**.

37 W.-C. Lee, B.-T. Lee, S. Lee, Y. S. Hwang, E. Jo, I.-C. Eom, S.-W. Lee and S.-O. Kim, Optimisation, evaluation and application of asymmetrical flow field-flow fractionation with single particle inductively coupled plasma mass spectrometry (SP-ICP-MS) to characterise silver nanoparticles in environmental media, *Microchem. J.*, 2016, **129**, 219–230, DOI: **10.1016/j.microc.2016.06.030**.

38 ISO/TS, *Nanotechnologies – Analysis of nano-objects using asymmetrical-flow and centrifugal field-flow fractionation*, 2018, **https://www.iso.org/obp/ui/#iso:std:iso:ts:**21362:ed-1:v1:en.

39 K. G. Wahlund and J. C. Giddings, Properties of an asymmetrical flow field-flow fractionation channel having one permeable wall, *Anal. Chem.*, 1987, **59**(9), 1332–1339, DOI: **10.1021/ac00136a016**.

40 E. R. Zylstra, Accumulation of wind-dispersed trash in desert environments, *J. Arid Environ.*, 2013, **89**, 13–15, DOI: **10.1016/j.jaridenv.2012.10.004**.

41 H. Zhang, D. Freitas and H. S. Kim, Identification of distinct nanoparticles and subsets of extracellular vesicles by asymmetric flow field-flow fractionation, *Nat. Cell Biol.*, 2018, **20**(3), 343, DOI: **10.1038/s41556-018-0040-4**.

42 G. Yohannes, M. Jussila, K. Hartonen and M. L. Riekkola, Asymmetrical flow field-flow fractionation technique for separation and characterization of biopolymers and bioparticles, *J. Chromatogr. A*, 2011, **1218**(27), 4104–4116, DOI: **10.1016/j.chroma.2010.12.110**.

43 C. Fuentes, H. Saari, J. Choi, S. Lee, M. Sjoo, M. Wahlgren and L. Nilsson, Characterization of non-solvent precipitated starch using asymmetrical flow field-flow fractionation coupled with multiple detectors, *Carbohydr. Polym.*, 2019, **206**, 21–28, DOI: 10.1016/j.carbpol.2018.10.100.

44 B. Meisterjahn, S. Wagner, F. von der Kammer, D. Hennecke and T. Hofmann, Silver and gold nanoparticle separation using asymmetrical flow-field flow fractionation: Influence of run conditions and of particle and membrane charges, *J. Chromatogr. A*, 2016, **1440**, 150–159, DOI: 10.1016/j.chroma.2016.02.059.

45 L. Sanchez-Garcia, E. Bolea, F. Laborda, C. Cubel, P. Ferrer, D. Gianolio, I. da Silva and J. R. Castillo, Size determination and quantification of engineered cerium oxide nanoparticles by flow field-flow fractionation coupled to inductively coupled plasma mass spectrometry, *J. Chromatogr. A*, 2016, **1438**, 205–215, DOI: 10.1016/j.chroma.2016.02.036.

46 K. A. Huynh, E. Siska, E. Heithmar, S. Tadjiki and S. A. Pergantisi, Detection and quantification of silver nanoparticles at environmentally relevant concentrations using asymmetric flow field-flow fractionation online with single particle inductively coupled plasma mass spectrometry, *Anal. Chem.*, 2016, **88**(9), 4909–4916, DOI: 10.1021/acs.analchem.6b00764.

47 J. Gigault, H. El Hadri, S. Reynaud, E. Deniau and B. Grassl, Asymmetrical flow field flow fractionation methods to characterize submicron particles: application to carbon-based aggregates and nanoplastics, *Anal. Bioanal. Chem.*, 2017, **409**(29), 6761–6769, DOI: 10.1007/s00216-017-0629-7.

48 M. Correia and K. Loeschner, Detection of nanoplastics in food by asymmetric flow field-flow fractionation coupled to multi-angle light scattering: possibilities, challenges and analytical limitations, *Anal. Bioanal. Chem.*, 2018, **410**(22), 5603–5615, DOI: 10.1007/s00216-018-0919-8.

49 H. Li, L. M. Lee, D. Yu, S. H. Chan and A. Li, An optimized multi-technique based analytical platform for identification, characterization and quantification of nanoplastics in water, *Talanta*, 2024, **272**, 125800, DOI: 10.1016/j.talanta.2024.125800.

50 T. Zarei, M. B. A. Colombo, E. C. Fuchs, H. L. Offerhaus, D. Gebauer and L. L. F. Agostinho, Characterization of nanoparticles in drinking water using field-flow fractionation coupled with multi-angle light scattering and inductively coupled plasma mass spectrometry, *Water*, 2024, **16**(17), 2419, DOI: 10.3390/w16172419.

51 M. Amde, Z. Q. Tan and J. Liu, Separation and size characterization of zinc oxide nanoparticles in environmental waters using asymmetrical flow field-flow fractionation, *Talanta*, 2019, **200**, 357–365, DOI: 10.1016/j.talanta.2019.03.074.

52 S. Chakraborty, R. Drexel, P. Bhadane, N. Langford, P. Dhumal, F. Meier and I. Lynch, An integrated multimethod approach for size-specific assessment of potentially toxic element adsorption onto micro- and nanoplastics: implications for environmental risk, *Nanoscale*, 2025, **17**(15), 9122–9136, DOI: 10.1039/d5nr00353a.

53 H. Hagendorfer, R. Kaegi, J. Traber, S. F. L. Mertens, R. Scherrers, C. Ludwig and A. Ulrich, Application of an asymmetric flow field flow fractionation multi-detector approach for metallic engineered nanoparticle characterization – Prospects and limitations demonstrated on Au nanoparticles, *Anal. Chim. Acta*, 2011, **706**(2), 367–378, DOI: 10.1016/j.aca.2011.08.014.

54 C. Sun, B. Zhang and Y. He, Parameter optimization of nanoparticle separation from domestic sewage by asymmetrical flow field-flow technology, *Water Purif. Technol*, 2018, **37**(10), 55–61, DOI: 10.15890/j.cnki.jsjs.2018.10.011.

55 Y. Mao, H. Li, X. Huangfu, Y. Liu and Q. He, Nanoplastics display strong stability in aqueous environments: Insights from aggregation behaviour and theoretical calculations, *Environ. Pollut.*, 2020, **258**, 113760, DOI: 10.1016/j.envpol.2019.113760.

56 Y. Liu, Z. Huang, J. Zhou, J. Tang, C. Yang, C. Chen, W. Huang and Z. Dang, Influence of environmental and biological macromolecules on aggregation kinetics of nanoplastics in aquatic systems, *Water Res.*, 2020, **186**, 116316, DOI: 10.1016/j.watres.2020.116316.

57 F. Wang and V. V. Tarabara, Pore blocking mechanisms during early stages of membrane fouling by colloids, *J. Colloid Interface Sci.*, 2008, **328**(2), 464–469, DOI: 10.1016/j.jcis.2008.09.028.

58 F. A. Monikh, N. Grundschober, S. Romeijn, D. Arenas-Lago, M. G. Vijver, W. Jiskoot and W. J. G. M. Peijnenburg, Development of methods for extraction and analytical characterization of carbon-based nanomaterials (nanoplastics and carbon nanotubes) in biological and environmental matrices by asymmetrical flow field-flow fractionation, *Environ. Pollut.*, 2019, **255**, 113304, DOI: 10.1016/j.envpol.2019.113304.

59 R. C. Murdock, L. Braydich-Stolle, A. M. Schrand, J. J. Schlager and S. M. Hussain, Characterization of nanomaterial dispersion in solution prior to *In vitro* exposure using dynamic light scattering technique, *Toxicol. Sci.*, 2008, **101**(2), 239–253, DOI: 10.1093/toxsci/kfm240.

60 Y. Dieckmann, H. Coelfen, H. Hofmann and A. Petri-Fink, Particle size distribution measurements of manganese-doped ZnS nanoparticles, *Anal. Chem.*, 2009, **81**(10), 3889–3895, DOI: 10.1021/ac900043y.

61 Z. Dong, Y. Qiu, W. Zhang, Z. Yang and L. Wei, Size-dependent transport and retention of micron-sized plastic spheres in natural sand saturated with seawater, *Water Res.*, 2018, **143**, 518–526, DOI: 10.1016/j.watres.2018.07.007.

62 A. Pradel, C. Catrouillet and J. Gigault, The environmental fate of nanoplastics: What we know and what we need to know about aggregation, *NanoImpact*, 2023, **29**, 100453, DOI: 10.1016/j.impact.2023.100453.

63 S. Li, H. Liu, R. Gao, A. Abdurahman, J. Dai and F. Zeng, Aggregation kinetics of microplastics in aquatic environment: Complex roles of electrolytes, pH, and

natural organic matter, *Environ. Pollut.*, 2018, **237**, 126–132, DOI: **10.1016/j.envpol.2018.02.042**.

64 I. Chowdhury, M. C. Duch, N. D. Mansukhani, M. C. Hersam and D. Bouchard, Colloidal properties and stability of graphene oxide nanomaterials in the aquatic environment, *Environ. Sci. Technol.*, 2013, **47**(12), 6288–6296, DOI: **10.1021/es400483k**.

65 X. Wang, N. Bolan, D. C. W. Tsang, B. Sarkar, L. Bradney and Y. Li, A review of microplastics aggregation in aquatic environment: Influence factors, analytical methods, and environmental implications, *J. Hazard. Mater.*, 2021, **402**, 123496, DOI: **10.1016/j.jhazmat.2020.123496**.

66 C. Schneider, M. Hanisch, B. Wedel, A. Jusufi and M. Ballauff, Experimental study of electrostatically stabilized colloidal particles: Colloidal stability and charge reversal, *J. Colloid Interface Sci.*, 2011, **358**(1), 62–67, DOI: **10.1016/j.jcis.2011.02.039**.

67 M. Baalousha, Y. Nur, I. Roemer, M. Tejamaya and J. R. Lead, Effect of monovalent and divalent cations, anions and fulvic acid on aggregation of citrate-coated silver nanoparticles, *Sci. Total Environ.*, 2013, **454**, 119–131, DOI: **10.1016/j.scitotenv.2013.02.093**.

68 A. M. El Badawy, K. G. Scheckel, M. Suidan and T. Tolaymat, The impact of stabilization mechanism on the aggregation kinetics of silver nanoparticles, *Sci. Total Environ.*, 2012, **429**, 325–331, DOI: **10.1016/j.scitotenv.2012.03.041**.

69 A. Sanchez-Cachero, N. Rodriguez Farinas, A. Rios and R. d. C. Rodriguez Martin-Doimeadios, Assessment by a multi-technique approach of PtNPs' transformations in waters under relevant environmental concentrations and conditions, *Sci. Total Environ.*, 2023, **861**, 160686, DOI: **10.1016/j.scitotenv.2022.160686**.

70 B. Meermann, A. L. Fabricius, L. Duester, F. Vanhaecke and T. Ternes, Fraction-related quantification of silver nanoparticles *via* on-line species-unspecific post-channel isotope dilution in combination with asymmetric flow-field-flow fractionation (AF4)/sector field ICP-mass spectrometry (ICP-SF-MS), *J. Anal. At. Spectrom.*, 2014, **29**(2), 287–296, DOI: **10.1039/c3ja50179e**.